# Assembly of Layered Monetite-Chitosan Nanocomposite and Its Transition to Organized Hydroxyapatite
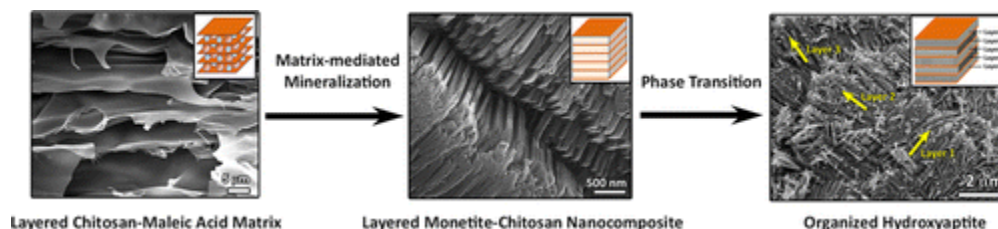
Qichao Ruan[a], David Liberman[a], Yuzheng Zhang[b], Dongni Ren[a], Yunpeng Zhang[b], Steven Nutt[b], and Janet Moradian-Oldak[a]*

[a] Center for Craniofacial Molecular Biology, Herman Ostrow School of Dentistry, University of Southern California, 2250 Alcazar Street, Los Angeles, California 90033, United States
[b] Mork Family Department of Chemical Engineering and Materials Science, University of Southern California, 3651 Watt Way, Los Angeles, California 90089, United States

* E-mail: joldak@usc.edu. Tel.: +1 323 442 1759. Fax: +1 323 442 2981.

**Abstract:**

Layered Chitosan-Maleic Acid Matrix — Matrix-mediated Mineralization → Layered Monetite-Chitosan Nanocomposite — Phase Transition → Organized Hydroxyaptite

Bioinspired synthesis of hierarchically structured calcium phosphate (CaP) material is a highly promising strategy for developing improved bone substitute materials. However, synthesis of CaP materials with outstanding mechanical properties still remains an ongoing challenge. Inspired by the formation of lamellar structure in nacre, we designed an organic matrix composed of chitosan and cis-butenediolic acid (maleic acid, MAc) that could assemble into a layered complex and further guide the mineralization of monetite crystals, resulting in the formation of organized and parallel arrays of monetite platelets with a brick-and-mortar structure. Using the layered monetite-chitosan composite as a precursor, we were able to synthesize hydroxyapatite (HAp) with multiscale hierarchically ordered structure via a topotactic phase transformation process. On the nanoscale, needlelike HAp crystallites assembled into organized bundles that aligned to form highly oriented

plates on the microscale. On the large-scale level, these plates with different crystal orientations were stacked together to form a layered structure. The organized structures and composite feature yielded CaP materials with improved mechanical properties close to those of bone. Our study introduces a biomimetic approach that may be practical for the design of advanced, mechanically robust materials for biomedical applications.

Key words: bioinspired matrix, monetite, hierarchical structure, hydroxyapatite, chitosan, maleic acid.

# 1. INTRODUCTION

Calcium phosphates (CaP) are important biomaterials in the fields of tissue engineering and drug delivery, because of their low toxicity, excellent biocompatibility, and osteoconductivity. For example, nanostructured CaP materials have been used in biomedical products such as scaffolds for bone regrowth,[1] bioactive coatings and composites,[2] carriers for drug delivery,[3] and bioactive fillers for the occlusion of exposed dentin tubules.[4] However, the application of conventional CaP materials as hard tissue substitutes has been largely restricted by their brittleness and low strength. Progress to reinforce their mechanical properties through incorporation of high-strength materials in the CaP matrix has been incremental.[5, 6] Therefore, there is a need for an effective alternative strategy to boost the mechanical properties of synthetic CaP materials in a way to broaden their application in the areas of repair of multiple fractures of long bones, or vertebral body substitution.[7]

The hierarchical structure of biological composites has inspired scientists to develop high-performance materials with superior properties and functionalities.[8-12] Natural structural

materials such as nacre, bone, and tooth exhibit excellent mechanical performance associated with their composition and unique hierarchical structures. For instance, the lamellar architectures in nacre and bone are well-known structures that provide these biocomposites with mechanical properties that far exceed those of their constituent materials.(13) Another prime example, tooth enamel, consists of densely packed arrays of elongated apatite crystals organized into an intricate interwoven structure.(14) Because of its unique architecture and dense mineral components, mature enamel possesses remarkably high elastic modulus and hardness, which are rarely achieved in artificial CaP materials.(15, 16) Thus, mimicking the structural features of such natural composites is a promising route to developing new structural materials with superior mechanical performance.(13, 16)

Over the past decade, efforts to synthesize CaP materials with bioinspired structures have relied on methods such as freeze casting,(17) vacuum-assisted filtration,(18) and biomimetic mineralization.(19, 20) In one such study, a bioinspired hydroxyapatite/poly(methyl methacrylate) composite with a nacre-mimetic lamellar structure was prepared by a bidirectional freezing method,(17) and in another, Li et al. used a vacuum-assisted-filtration method to combine CaP plates with amyloid fibrils to generate a hybrid nanocomposite with bone-mimetic features.(18) Bioinspired CaP materials with bone-mimetic or enamel-like structures have also been synthesized through matrix-regulating mineralization of apatite nanocrystals with the assistance of peptides,(21, 22) proteins,(23-25) protein-inspired polymers,(26, 27) block copolymers,(28, 29) self-assembled liquid crystals,(19, 20) and other organic additives.(30, 31) These promising studies illustrate steps toward the formation of intricate structures at limited scale, although synthesis of bioinspired CaP materials with the architectural features over multiple length scales remains a great challenge. Another promising route to achieve hierarchical structures in CaP materials involves the use of a

precursor crystal as a template. For example, based on the structural resemblance between monetite (dicalcium phosphate anhydrous, DCPA, $CaHPO_4$) and hydroxyapatite (HAp, $Ca_5(PO_4)_3OH$) crystals, monetite was shown to be an effective precursor in the preparation of various nanostructured hydroxyapatite crystals.(32-34) Using macrosized crystals as a template, Liu et al. synthesized ordered HAp structures via a phase transformation from monetite.(35) This result demonstrated the feasibility of mimicking hierarchical designs of natural structures via a phase transformation from precursor crystals. However, the time-consuming preparation of the macro-sized monetite precursor (3 to 6 months) challenged its suitability for broader applications. Generating multilevel hierarchy is still a huge challenge in the fabrication of HAp from the direct transformation of a single monetite crystal.

In the present study, we report a biomimetic strategy, inspired by the formation of brick-and-mortar structure in nacre, to generate a layered monetite-based composite that can further transform into a HAp-chitosan composite with a multilevel hierarchical structure. In nacre, the orderly layered structure forms under the mediation of an organic matrix composed of β-chitin, silklike proteins, and acidic glycoproteins rich in aspartic acid (Asp).(36-38) Among these components, the oriented fibrils of β-chitin play an important role in regulating the crystal orientation, and the Asp-rich proteins are believed to interact both with the β-chitin substrate and the growing crystals.(36) Considering the critical functions of β-chitin and acidic proteins, our strategy starts with the rational design of an organic medium composed of chitosan and cis-butenediolic acid (maleic acid, MAc) to mimic the function of nacreous matrix and to generate an ordered layered structure. Chitosan is a deacetylated derivative of chitin usually used to study the crystallization process instead of chitin, owing to its soluble properties in acidic media. Experiments have shown that chitosan scaffolds are capable of

promoting the formation of randomly spherelike, rodlike, or platelike CaP crystals,(39-41) yet no observable higher-order structure has been reported in these materials, perhaps because of the absence of orderly assembly of the pristine chitosan molecules.(42) To overcome this problem, here we introduced a dicarboxylic MAc molecule that could serve as a cross-linking agent and lead to the intermolecular assembly of an organized matrix (Figure 1, step (i)). In addition to the cross-linking capability, the carboxyl functional groups of MAc could also afford the matrix with interactive sites to nucleate the monetite crystals and mediate the formation of a layered structure (Figure 1, step (ii)). Using this layered monetite precursor, we were able to synthesize a hierarchical composite with orderly bundlelike structures on the nanoscale as well as layered organization on the microscale through a controlled phase transformation process (Figure 1, step (iii)). These hierarchical structures are expected to provide CaP materials with improved mechanical properties and potential for future hard tissue engineering applications.
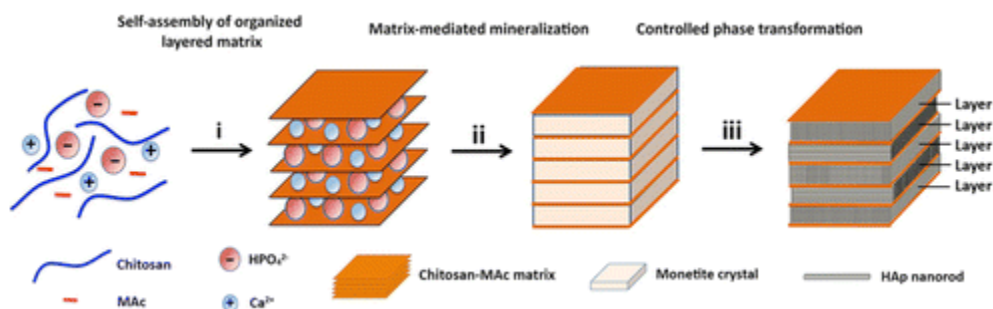


*Figure 1. Schematic representation of the pathway followed to fabricate multilevel organized CaP-based composite.*

## 2. MATERIALS AND METHODS

### 2.1. Analyses of Chitosan-MAc Matrix

To investigate the assembly of the layered matrix, we prepared the chitosan-MAc solution by dissolving 0.25 g of chitosan (medium molecular weight, 75–85% deacetylated, Sigma–Aldrich) and

0.1 g of maleic acid (MAc, Sigma–Aldrich) in 25 mL of deionized water containing 0.72 mL of acetic acid under magnetic stirring, and the pH value was adjusted to 3.5 with 1 M NaOH. The solid phase of chitosan-MAc matrix was obtained by lyophilization for scanning electron microscopy (SEM), X-ray diffraction (XRD), and Fourier transform infrared spectroscopy (FTIR) studies. For circular dichroism (CD), atomic force microscopy (AFM) and transmission electron microscopy (TEM) studies, 0.1 mL of chitosan-MAc solution was diluted with 0.9 mL deionized water. The TEM sample was prepared by depositing a droplet of the diluted chitosan-MAc solution onto a TEM grid and then staining it with a droplet of a 0.1 wt % phosphotungstic acid aqueous solution.

## 2.2. Preparation of Layered Monetite-Chitosan-MAc Composite

Six grams of urea, 0.25 g of chitosan (medium molecular weight, 75–85% deacetylated, Sigma–Aldrich) and 0.1 g of maleic acid (MAc, Sigma–Aldrich) were dissolved in 25 mL of deionized water containing 0.72 mL of acetic acid under magnetic stirring. Then, 0.3 g of $NaH_2PO_4$ and 0.614 g of $CaCl_2 \cdot 2H_2O$ were dissolved into the solution under vigorous stirring for 2 h, and the pH value was adjusted to 3.5 with 1 M NaOH. Next, the reaction solution was heated in a water bath at 70 °C for 4.5 h, then allowed to cool down to room temperature naturally. Following the reaction, the obtained suspension was centrifuged and washed with distilled water and anhydrous ethanol several times. Finally, the sample was frozen on dry ice and lyophilized for 16 h.

## 2.3. Preparation of Organized HAp-chitosan-MAc Composite via Phase Transition

Layered monetite-chitosan-MAc composite (0.15 g) was dispersed in 15 mL of NaOH solution (0.1 M, pH 13) and kept in a water bath under vigorous stirring at 70 °C for 5 min. The suspension was then immediately centrifuged and washed with distilled water and anhydrous ethanol several times. Finally, the sample was frozen on dry ice and lyophilized overnight.

## 2.3. Preparation of Calcium Phosphate Tablets

The CaP tablets were prepared by pressing the layered monetite-chitosan-MAc or organized HAp-chitosan-MAc composite in a stainless steel mold under a pressure of 10 MPa at 130 °C for 48 h.

## 2.3. Characterization

SEM imaging was performed in a JSM-7001F field emission scanning electron microscope (JEOL, Peabody, MA) operating at an accelerating voltage of 5–15 kV. XRD patterns were recorded by a Rigaku diffractometer with Cu Kα radiation ($\lambda$ = 1.542 Å) operating at 70 kV and 50 mA with a step size of 0.02°, at a scanning rate of 0.1°/sec in the 2θ range 10–60°. TEM images were obtained on a JEOL JEM-2100 microscope using an accelerating voltage of 200 kV. CD spectropolarimetry was performed using a J-815 spectropolarimeter (JASCO, Easton, MD). The spectra were recorded between 190 and 260 nm with a step size of 0.5 nm and a scan rate of 50 nm/min. AFM images were obtained by using a NanoScopeIIIa scanning probe microscope system (Digital Instruments, Tonawanda, NY) with a tapping mode etched silicon probe (model OTESPA-10) in air at scanning rates of 0.5–1.0 Hz for different resolutions. FTIR spectra were acquired from a Nicolet 4700 Spectrometer with a Gladi-ATR diamond crystal accessory. Thermogravimetry (TGA) analysis was performed on a Q5000 IR (TA Instruments, New Castle, DE) with a heating rate of 50 °C/min, under an air flow of 20 mL/min from 30 to 900 °C. The hardness and elastic modulus were measured at 25 test points in each sample ($n$= 3) using a nanoindenter (Agilent-MTS XP) with a Berkovich tip.

## 2.3. Statistical Analysis

The experiments were conducted in triplicate and the data were expressed as mean ± standard deviations. Student's $t$ test was applied to identify differences in the hardness and elastic modulus

between layered monetite-based composite and hierarchical HAp-based composite. The differences were considered statistically significant at $p < 0.05$ and highly significant at $p < 0.001$. All the statistical analyses were carried out using Origin 8.0 (Origin lab, Northampton, MA) and Microsoft Office Excel 2007.

# 3. RESULTS AND DISCUSSION

## 3.1. Assembly of Organized Chitosan-MAc Matrix

Unlike the chitin in nacre matrix, chitosan alone does not form an organized structure because it lacks the acetylamide groups that contribute to hydrogen bonding during the self-assembly of chitin.[42] In our study, only irregularly spherical-like morphology can be observed when examining pure chitosan (Figure 2a, b). Inspired by the critical role of intermolecular interaction in chitin assembly, we included maleic acid (MAc) into the chitosan matrix to provide an interactive cross-linker and facilitate the orderly assembly of the organic matrix.

Figures 2c, d show the sheetlike morphology of the organic matrix composed of chitosan and MAc. These chitosan-MAc sheets are stacked in parallel layered structures similar to the organized structures seen in nacreous matrix.[43] In addition, the XRD pattern of chitosan-MAc matrix displays a diffraction peak at a spacing of 0.37 nm (Figure 2e), representing short-range order in the chitosan-MAc molecular complex (Figure 2f). These observations demonstrate the ordered coassembly of chitosan-MAc matrix due to the specific interaction between chitosan and MAc, which was further confirmed by FTIR. Compared with the FTIR spectra of pure chitosan or MAc, the COO– stretch vibration band shifted from 1703 to 1710 cm$^{-1}$ in the spectra of chitosan-MAc mixture (Figure 3a), and the N–H bending vibration band shifted from 1581 to 1512 cm$^{-1}$ (Figure 3b).
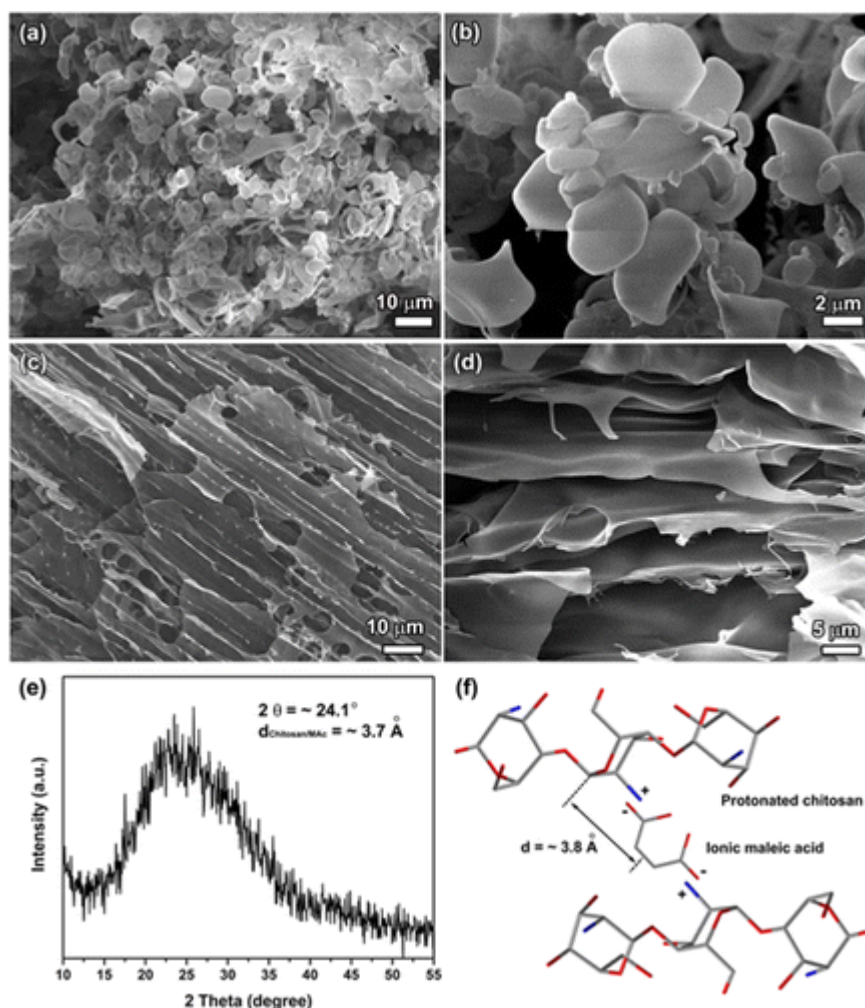
*Figure 2. SEM images of (a, b) pure chitosan matrix and (c, d) organized chitosan-MAc matrix: (a) top view, (b) side view. (e) XRD pattern of chitosan-MAc matrix. (f) Schematic representation of interaction between chitosan and MAc. The molecular model was established by ChemBio Ultra 11.0. The distance between the molecules was estimated using the typical bond lengths and angles. Blue in the chitosan chain and Red in the MAc molecule represent the charged amine and carboxyl groups, respectively.*

*Figure 3. (a, b) FTIR spectra of chitosan (blue), MAc (red), and chitosan-MAc matrix (gray) in the absence of calcium in (a) the C=O stretch and (b) the N–H bending regions. (c) CD spectra of chitosan and chitosan-MAc matrix at pH 3.5.*

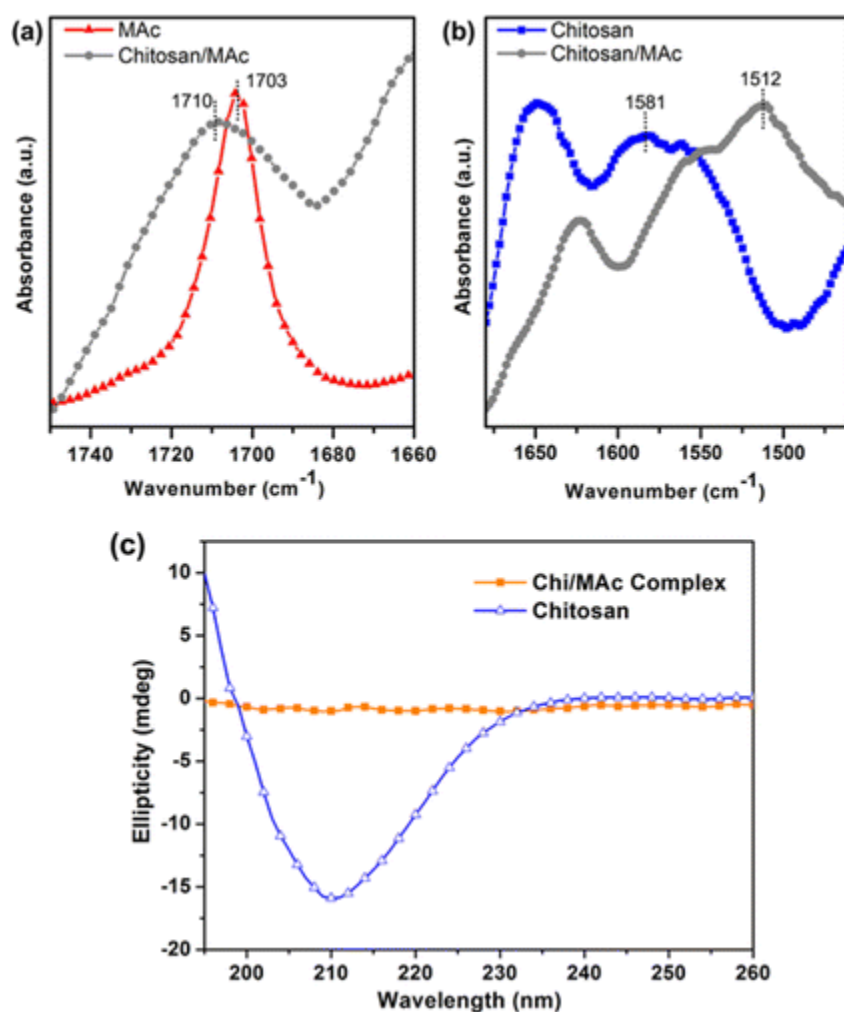These shifts indicate a strong interaction between the charged carboxyl and amine groups.(42, 44, 45) Indeed, under our experimental conditions ($3.5 < pH < 4.5$), the amine groups of chitosan ($pK_a = 6.5$) are protonated to form positively charged chains.(46) Simultaneously, the two carboxyl ends of MAc ($pK_a = 1.92$) are fully ionized.(47) As a result, the chitosan chains can be cross-linked by MAc molecules through hydrogen bonding and electrostatic interactions between the positively charged amine groups and the negatively charged carboxyl groups (Figure 2f). The specific chitosan-

MAc interaction is expected to cause a conformational change in the chitosan molecule, which is confirmed by the circular dichroism (CD) spectropolarimetry. As shown in Figure 3c, the CD spectrum of pure chitosan in aqueous solution (pH 3.5) has a broad negative CD band located at about 210 nm, corresponding to the n → π* electronic transition of the -NH–CO- chromophore of GlcNAc (N-acetyl-d-glucosamine) units.(48) After adding MAc to the chitosan solution, the negative dichroic signal of chitosan is absent (Figure 3c), indicating a distinct change in the chromophore environments of the GlcNAc units due to the interaction between chitosan and MAc.(49) This conformational change may give rise to an anisotropic ligand distribution in the chitosan-MAc complex that could further assist in the assembly of an organized matrix.(50, 51)

The assembly states of pure chitosan and chitosan-MAc matrix were revealed by tapping mode atomic force microscopy (AFM) and transmission electron microscopy (TEM) under the conditions described in Figure 3. Without MAc, the chitosan chains tend to aggregate into randomly distributed nanoparticles with a size of ∼30 nm due to hydrophobic or solvophobic interactions (Figure 4a, c), as proposed elsewhere.(52-55) In contrast, following addition of MAc we could observe linear chains of ∼50 nm nanoclusters in the chitosan-MAc matrix (arrows in Figure 4b, d). We speculate that this spontaneous linear assembly depends on an equilibrium between various attractive and repulsive interactions, such as hydrophobic interaction, van der Waal's attraction, hydrogen bonding and electrostatic repulsion.(56, 57) The attractive forces favor more contact between nanoparticles and drive the formation of compact aggregates, although electrostatic repulsion acts as a key driving force to form anisotropic self-assemblies of 1D chains.(58) The insertion of ionized MAc molecules into a chitosan system may dramatically disrupt the hydrophobic force within a close distance.(58) As a result, the repulsion between neighboring chitosan-MAc nanoparticles tends to force these

molecules into an ordered assembly to evenly distribute their charges. This process eventually leads to the formation of chitosan-MAc sheets that further stack into a layered structure. Based on the results discussed here (Figures 2–4), the self-assembly process of layered chitosan-MAc matrix is schematically presented in Figure S1. Using this chitosan-MAc matrix, we were able to further construct an orderly, layered monetite composite.
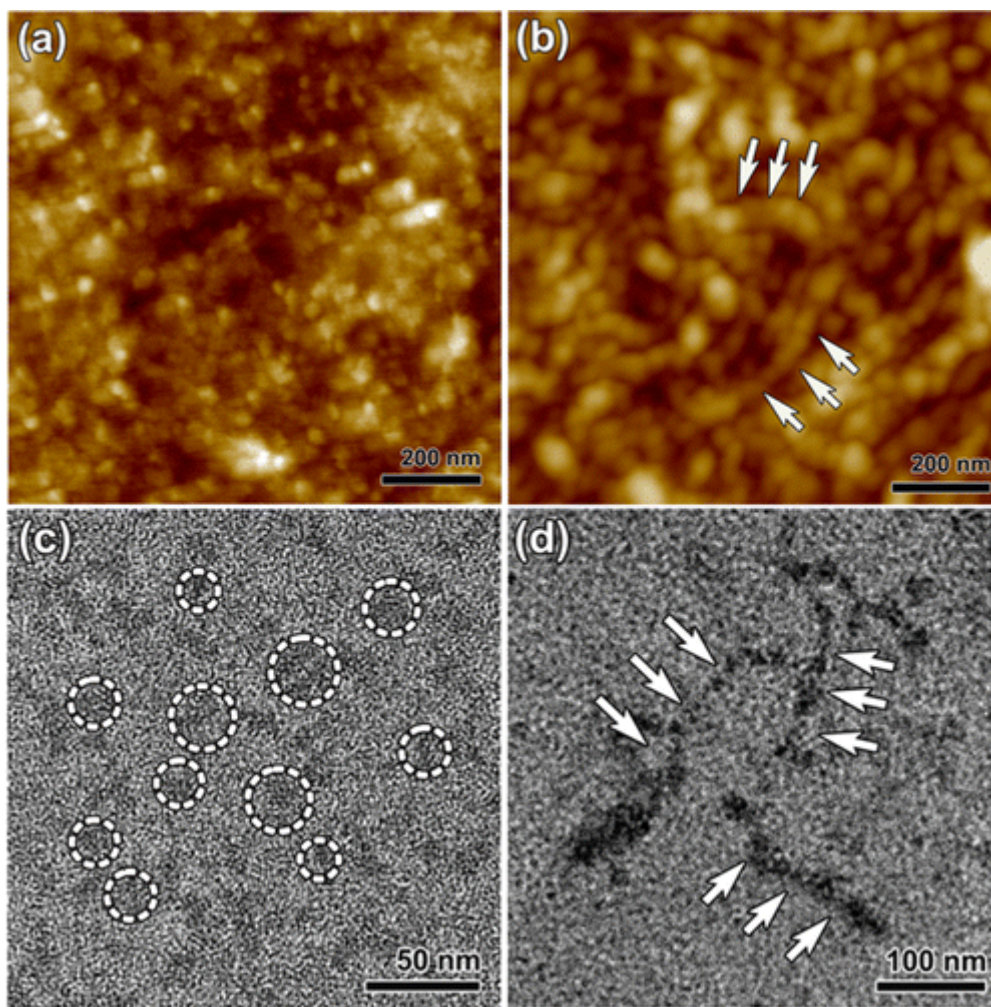


*Figure 4. (a, b) AFM and (c, d) TEM images of (a, c) pure chitosan and (b, d) organized chitosan-MAc matrix.*

J. Moradian-Oldak, Q. Ruan, D. Liberman, Y. Zhang, D. Ren, Y. Zhang, and S. Nutt, **"Assembly of Layered Monetite-Chitosan Nanocomposite and Its Transition to Organized Hydroxyapatite: An Alternative to Bone Substitute Material"** ACS Biomaterials Sci & Engrg 2 [6] 1049-58 (2016) **DOI: 10.1021/acsbiomaterials.6b00164**

## 3.2. Assembly of Layered Monetite-Chitosan-MAc Composite

To prepare a calcium phosphate composite with an orderly layered structure, we adopted a wet-chemical precipitation method in the presence of a chitosan-MAc mixture. The resulting calcium phosphate products exhibited a brick-and-mortar structure (Figure 5a–d), in which calcium phosphate platelets with a thickness of ∼100 nm were bound together by the organic binder (arrows in Figure 5c). High-resolution transmission electron microscopy (HRTEM) and corresponding fast Fourier transform (FFT) images provide further insight into the structural details of the calcium phosphate platelets (Figure 5e). The interplanar distances measured in segments of HRTEM micrograph were 0.250 and 0.289 nm, corresponding to the $(0\bar{2}2)$ and $(021)$ planes of monetite crystals (JCPDS Card: 71–1759), respectively. The corresponding FFT pattern further confirms that the calcium phosphate platelet has a monetite polymorph (inset in Figure 5e) imaged along the [200] direction, indicating that the facet planes of the monetite platelets are (200).

This crystallographic characterization and composition of the layered composite were further confirmed by XRD and energy dispersive X-ray spectroscopy (EDS) (Figure 5f and Figure S2a). The resulting diffractogram shows that the products are mainly composed of monetite crystals (JCPDS Card: 71–1759). A strong 200 diffraction peak indicates a preferred (200) orientation of the monetite platelets in accordance with the above HRTEM analysis. In addition, a broad diffraction peak around $2\theta = 20°$ may be ascribed to the presence of organic matrix in the layered composite. The TG curve in Figure 5g shows that the total weight loss of monetite-chitosan composite is 17.2% in the range of 100–900 °C, whereas pure monetite should give a weight loss of 6.6% when it is decomposed completely $(2CaHPO_4 \xrightarrow{\Delta} Ca_2P_2O_7 + H_2O).$(60) Aside from the weight loss caused by

the decomposition of monetite, the additional weight loss of ~10.6% corresponds to loss of water

and the organic component. The structural and compositional analyses indicate that the products

synthesized in the chitosan-MAc matrix contain monetite with an organized, layered arrangement.
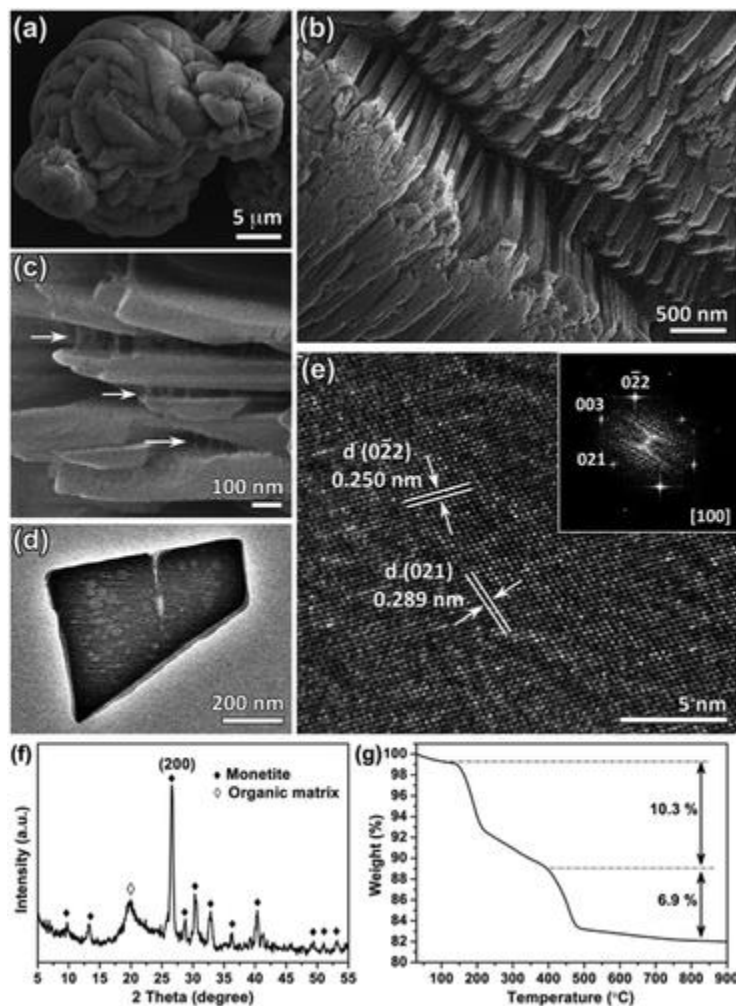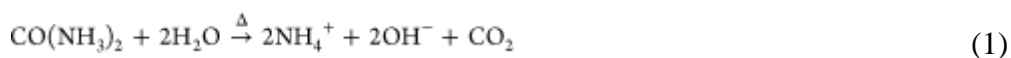


*Figure 5. (a–c) SEM images of the orderly layered monetite-chitosan-MAc composite. (d) TEM and (e) HRTEM images of a monetite nanosheet. Inset: FFT pattern corresponding to e. (f) XRD pattern and (g) TG curve of the layered monetite-chitosan-MAc composite.*

To investigate the assembly process of the layered monetite-chitosan-MAc composite, the

pH of the reaction system and the product morphology were monitored at different reaction times

(Figure 6). When the solution contained no $Ca^{2+}$, the pH increased with prolonged reaction time due

to the hydrolysis of urea (dotted line in Figure 6a). In contrast, a reduction in pH was observed in the reaction solution when the reaction time increased to 1 h (solid line in Figure 6a). Moreover, the addition of $Ca^{2+}$ in the reaction solution resulted in lower pH values because of the nucleation of monetite in the system. To diminish the effect of urea hydrolysis on the pH change and better understand the crystallization process, the pH difference ($\Delta$pH) between the solutions with and without $Ca^{2+}$ was calculated at different reaction times. As shown in Figure 6b, the $\Delta$pH rose from 0 to 0.5 within the first hour of reaction and dropped to ~0.3 when reaction time reached 2 h. After that, only slight changes were seen in the $\Delta$pH. On the basis of these observations, the possible reaction process in the chitosan-MAc matrix can be inferred as follows (eqs 1–3).

$$CO(NH_3)_2 + 2H_2O \xrightarrow{\Delta} 2NH_4^+ + 2OH^- + CO_2 \tag{1}$$

$$H_2PO_4^- + OH^- \rightarrow HPO_4^{2-} + H_2O \tag{2}$$

$$Ca^{2+} + HPO_4^{2-} \rightarrow CaHPO_4 \tag{3}$$

$H_2PO_4^-$ is dominant in the initial reaction solution with a pH of 3.5. As reaction time increases, the pH gradually increases due to the hydrolysis of urea (eq 1), leading to a conversion of $H_2PO_4^-$ to $HPO_4^{2-}$ (eq 2).[61] When the concentration product of $Ca^{2+}$ and $HPO_4^{2-}$ is larger than the Ksp of monetite, the monetite starts crystallizing in the solution (eq 3). Meanwhile, the nucleation of crystals leads to a decrease in the pH of the reaction solution because of the consumption of $Ca^{2+}$ and $OH^-$ (eqs 2 and 3). When the reaction time is increased to 1 h, white precipitation of monetite is formed in the solution. The products obtained at this time consist of monetite platelets assembled in an orderly layered structure (Figure 6c). After 2 h, there are no significant changes in $\Delta$pH, indicating that the main reaction in the solution is the assembly of monetite crystals. At this stage, the initially

formed crystals (Figure 6c) further stack and aggregate together (Figure 6d) and eventually form
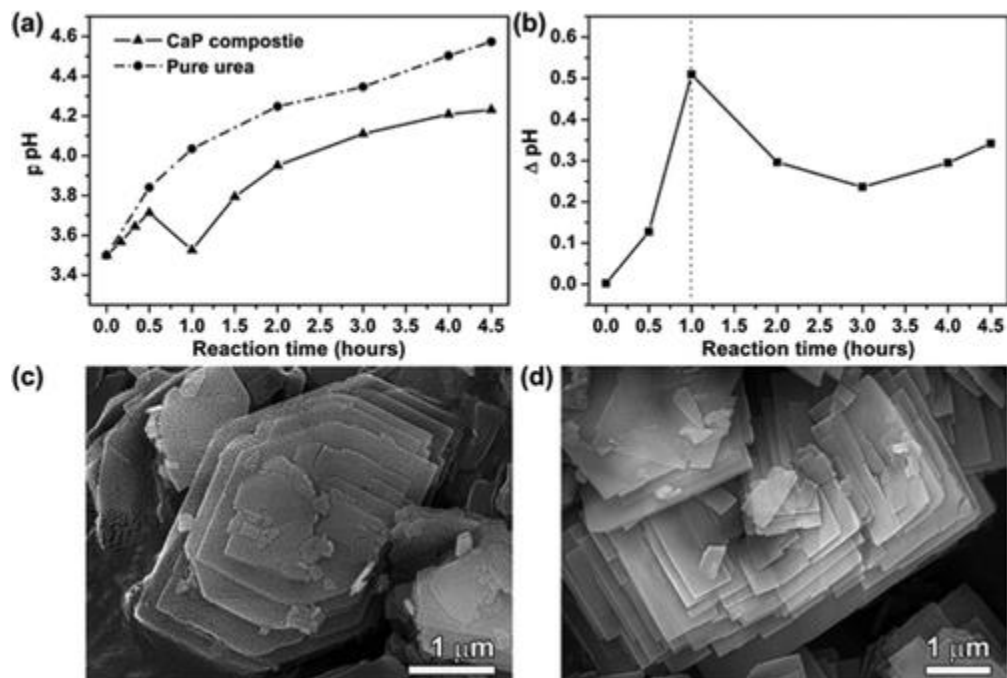
~30 μm spheres, as shown in Figure 5a.



*Figure 6. (a) pH values of reaction solution without (dotted line) and with (solid line) $Ca^{2+}$ at different reaction times. (b) pH difference (ΔpH) between the solutions with and without $Ca^{2+}$ at different time points. (c, d) SEM images of the products collected at (c) 1 and (d) 2 h.*

We can further consider the role of the chitosan-MAc mixture in this assembly mechanism. We did not observe any layered structure at any point during the reaction process in the absence of either chitosan or MAc. In a comparative experiment without chitosan and MAc, the monetite produced from precipitation formed plate-shaped structures with a width of 5–10 μm (Figure S3a). Only platy monetite crystals were formed in the absence of MAc (Figure S3b), and only porous HAp was produced in the absence of chitosan (Figure S3c). Other evidence for the critical role of the chitosan-MAc matrix is provided in a series of experiments in which we examined the thickness of monetite crystals as a function of chitosan and MAc concentration. Remarkably, changes in the

thickness of monetite crystals were observed upon altering the concentration of chitosan-MAc matrix in a dose dependent manner. As shown in Figures 7 and 5b, the thickness of monetite crystals decreased from ∼200 nm to ∼100 nm and ∼50 nm when the concentration of chitosan increased from 0.5% (m/v) to 1% (m/v) and 3% (m/v). (Note: the mass ratio of chitosan to maleic acid was kept steady at 2.5.) These observations suggest that the chitosan-MAc mixture is crucial to the construction of orderly layered monetite composite.
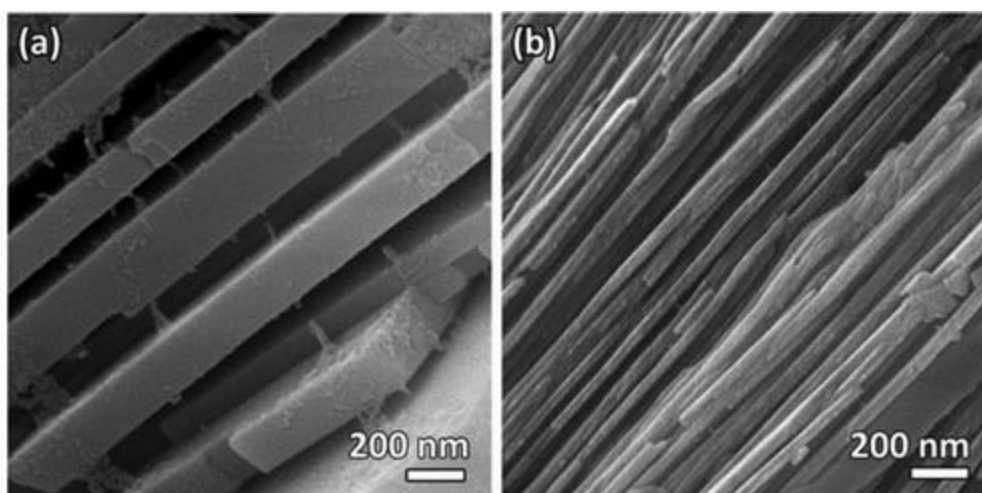


*Figure 7. SEM images of the layered monetite-chitosan-MAc composites formed in chitosan-MAc matrix with different concentrations: (a) 0.5% (m/v) chitosan and 0.2% (m/v) maleic acid; and (b) 3% (m/v) chitosan and 1.2% (m/v) maleic acid.*

It is noteworthy that the pH values (3.5 < pH < 4.5) of the reaction solution are in between the $pK_a$ values of maleic acid (1.92) and chitosan (6.5) throughout the reaction process. As a result, the protonated amine groups and ionized carboxyl groups remain active and interact with each other, leading to a persistent assembly and function of the chitosan-MAc matrix during the formation of layered monetite composite. Similar to the formation of nacre,[37, 38] the chitosan-MAc layers not only function as a structural framework, but also provide a charged carboxylate surface that plays an important role in inducing nucleation and interacting with forming crystals. The negatively

charged carboxyl groups of the chitosan-MAc complex are preferentially adsorbed on the calcium-rich (100) surface of crystals to stabilize and confine the formation of monetite platelets. The interaction between the organic complex and the calcium ions can be verified by the appearance of a characteristic FTIR vibration of COO-Ca at 1466 cm–1 (Figure 8).(32) The proposed formation process of layered monetite-chitosan-MAc composite under the mediation of chitosan-MAc matrix is summarized as follows (Figure S4). First, the negatively charged carboxyl groups of chitosan-MAc matrix act as active sites to interact with calcium and phosphate ions, inducing the heterogeneous nucleation of monetite. Then, guided by the chitosan-MAc matrix template, the monetite platelets are formed in between the layers of the chitosan-MAc scaffold, and finally grow in an organized manner into an orderly layered structure.
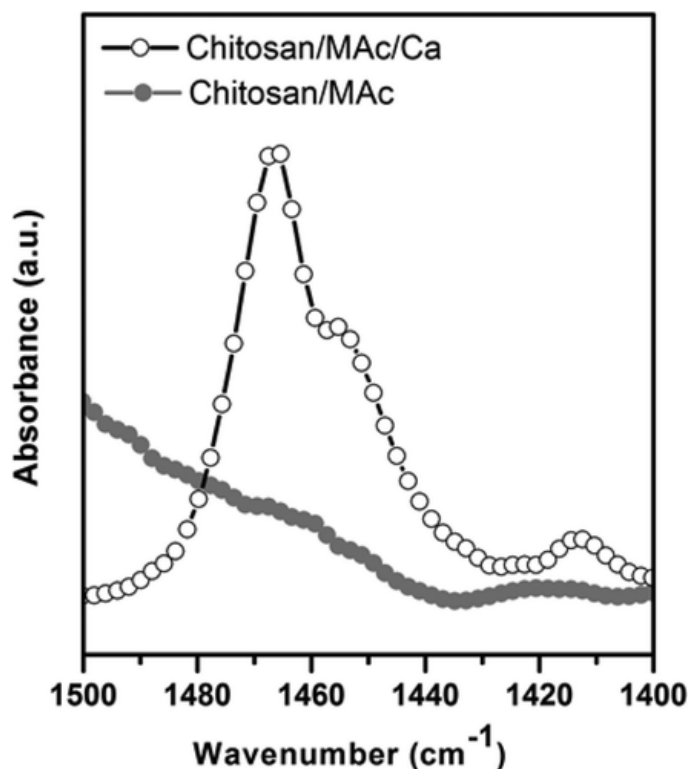


*Figure 8. FTIR spectrum of the chitosan-MAc-Ca$^{2+}$ complex.*

## 3.3. Synthesis of Organized HAp-Chitosan-MAc Composite via Phase Transition

Using the layered monetite-chitosan-MAc composite, we were able to fabricate an organized HAp-chitosan-MAc composite via a phase transformation in an alkali solution at 70 °C. XRD and EDS results confirmed that hydroxyapatite (JSPDS Card: 09–0432) was obtained after immersing the monetite-chitosan composite in a 0.1 M NaOH (pH 13) solution for 5 min (Figure S5). This process produced a multilevel ordered structure, as shown in Figure 9a–c. On the nanoscale, needlelike HAp crystallites with a diameter of ∼25 nm assembled into organized bundles (inset in Figure 9b). On the microscale, these HAp bundles aligned to form highly oriented plates about 2 μm in width and 4 μm in length (Figure 9b). Most interestingly, on the larger-scale level, these HAp plates with different crystal orientations stacked to form a layered structure (arrows in Figure 9c). A typical layer consisted of a HAp plate with an estimated thickness of ∼100 nm, which was inherited from the monetite precursor. Clearly, the layered arrangement of the monetite precursor was preserved to some extent during the phase transformation.

During the phase transformation from monetite to HAp, the ordered nanostructure can only be obtained through a topotactic solid–solid transition under highly alkaline conditions ($10CaHPO_4 + 6OH^- \rightarrow Ca_{10}(PO_4)_6(OH)_2 + 4PO_4^{3-} + 10H_2O$).[35] Specifically, the highly alkaline conditions generate a strong driving force that compels the ions to move and rearrange inside the crystal, resulting in a spatially periodic nucleation of HAp seeds and formation of well-arranged HAp nanoneedles on the monetite surface. However, the structural stress induced by dehydration and the movement of ions during the transition from monetite to HAp can cause changes to the crystal morphology and collapse of the layered structures.[34, 62] Thus, a major challenge associated with synthesis of hierarchical HAp in the present study was to preserve the layered arrangement on a

larger-scale level during the phase transformation from monetite composite to HAp. One way to overcome this problem is to use an organic matrix that can protect the organized layered structures. For example, by using different biomacromolecules and surfactants, the crystal morphology can be maintained during the phase transformation from OCP to HAP because of the interaction between organic molecules and crystals.(61) In a similar way, the chitosan-MAc matrix was expected to preserve the hierarchical architecture of crystals during the monetite-HAp transition by interacting with the crystal surface as discussed above.
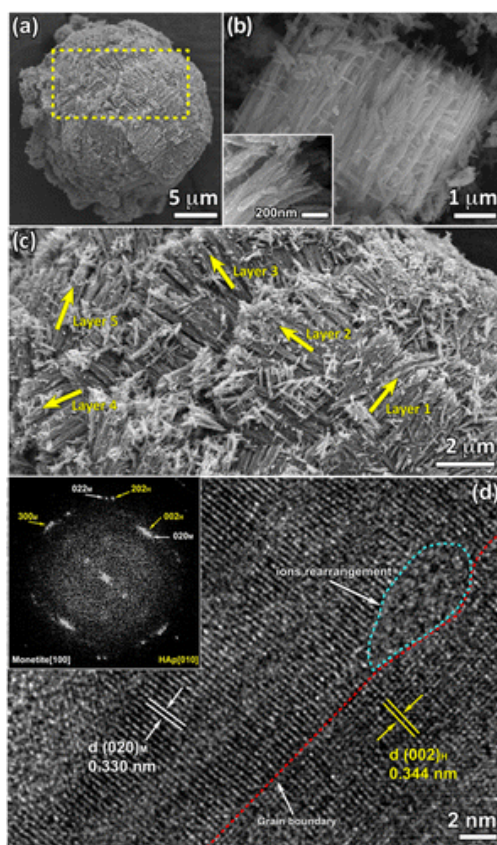


*Figure 9. Organized HAp-chitosan-MAc composite formed from phase transformation of layered monetite-chitosan-MAc composite. (a–c) SEM images of HAp-chitosan-MAc composite. Inset image in b shows the SEM image of an organized bundle. Arrows in (c) indicate different layers (stacks of HAp plates) in the HAp-chitosan-MAc composite. (d) HRTEM images of an isolated crystal from the HAp-chitosan-MAc composite. Inset: FFT pattern corresponding to d.*

Given all these considerations, we ascribe the formation of our hierarchical HAp to a topotactic solid–solid transformation under the mediation of the chitosan-MAc matrix. The intraparticle topotactic transition was revealed by HRTEM and FFT analysis. Figure 9d depicts a HRTEM image of a single crystal of hierarchical HAp-chitosan composite obtained from the transformation of a monetite crystal, which clearly exhibits the lattice fringes of the (002) plane of the HAp (d= 0.344 nm), as well as the (020) plane of the monetite (d = 0.333 nm). Furthermore, we can observe an amorphous region located at the monetite-HAp boundary (Figure 9d), probably indicating ion rearrangement inside the crystal.(62) Additionally, the corresponding FFT image shows two different patterns containing both HAp and monetite spots (inset in Figure 9d). Note that the FFT spots of HAp and monetite are projected along the [010] and [100] axes, respectively, and the spots indexed as monetite (020) and HAp (002) nearly overlap, indicating that the (002) planes of HAp are nearly parallel to the (020) planes of the monetite crystals. These results suggest that the HAp crystals form on the (100) face of the $CaHPO_4$ single crystals and orient along the b-axis of $CaHPO_4$ because of the similarity of the $CaHPO_4$ and HAp crystal structures (Figure S6). As a result, the (010) plane of $CaHPO_4$ may transform into the (001) face of HAp, as indicated by HRTEM and FFT analysis (Figure 9d), leading to the eventual formation of HAp with bundle-like structure on the nanoscale. In addition, the chitosan-MAc matrix is stable on the crystal surface because of the low solubility of chitosan under alkaline conditions. Because of the protective effect of the chitosan-MAc matrix, the orderly layered structure of monetite-chitosan composite is inherited from the layered precursor during the topotactic phase transformation from monetite to HAp.

## 3.4. Mechanical Properties of Organized CaP-Based Composites

Because the poor mechanical properties of conventional CaP materials limit their application to non- or moderate load-bearing applications, improving their strength is of great interest. From a clinical point of view, an ideal CaP bone substitute material should have mechanical properties similar or superior to those of the bone tissue being replaced. To evaluate the mechanical properties of the synthetic CaP-based composites, we prepared bulk tablets via a simple hot-pressing process using layered monetite-chitosan-MAc and organized HAp-chitosan-MAc composites as the building blocks (Figure S7) and assessed the elastic modulus and hardness of these tablets by nanoindentation. As shown in Table 1, the elastic modulus and hardness of the tablets prepared from layered monetite-chitosan-MAc composite were measured to be $8.78 \pm 0.59$ and $0.31 \pm 0.16$ GPa, respectively, which are greater than those of conventional bone substitute materials reported in the literatures.[63, 64] For example, the elastic modulus of the monetite-chitosan-MAc tablet was nearly 16 times higher compared to that of conventional CaP cement ($0.55 \pm 0.09$ GPa).[64] By achieving a multilevel ordered structure, the elastic modulus and hardness of the tablets obtained from organized HAp-chitosan-MAc composite were significantly greater, $12.82 \pm 3.74$ GPa ($p < 0.001$) and $0.40 \pm 0.17$ GPa ($p < 0.05$), respectively. Remarkably, the elastic modulus of HAp-chitosan-MAc composite tablets was comparable to that of bone ($12.7 \pm 1.7$ GPa for cancellous bone and $12.9 \pm 2.2$ GPa for cortical bone)[63] and human dentin (11.59–16.33 GPa).[17] This improved mechanical performance could be explained by the extrinsic crack bridging and crack deflection in these hierarchical CaP composite materials.[13] Specifically, the chitosan-MAc matrix, acting as viscoelastic glue, generates limited deformation between the crystals, thereby allowing the relief of locally high stresses. In addition, the hierarchical structure could toughen the CaP materials by

deflecting the crack path from the plane of maximum tensile stress. The improved mechanical properties of the hierarchical CaP materials, together with their well-known biocompatibility and osteoconductivity, indicate the great potential for hard tissue engineering applications.

*Table 1. Comparison of the Hardness and Elastic Modulus of Reported Bone Substitute Materials, Organized CaP-Based Composites, And Natural Biological Materials[a]*

| CaP-based materials | | hardness (GPa) | elastic modulus (GPa) | ref |
|---|---|---|---|---|
| conventional CaP materials | conventional CaP cement | | $0.55 \pm 0.09$[b] | (63) |
| | fiber reinforced CaP cement | | $1.03 \pm 0.28$[b] | (63) |
| | bioactive CaP substitute | 0.24–0.27[c] | 3.6–5.2[c] | (64) |
| biological CaP materials | human dentine | 0.52–0.91[c] | 11.59–16.33[c] | (15) |
| | Cancellous bone | $0.63 \pm 0.11$[c] | $12.7 \pm 1.7$[c] | (64) |
| | cortical bone | $0.89 \pm 0.16$[c] | $12.9 \pm 2.2$[c] | (64) |
| organized CaP-chitosan-MAc composite materials | layered monetite-chitosan-MAc composite tablet | $0.31 \pm 0.16$[c] | $8.78 \pm 0.59$[c] | |
| | organized HAp-chitosan-MAc composite tablet | $0.40 \pm 0.17$[c],* | $12.82 \pm 3.74$[c],*** | |

a*$p < 0.05$ and ***$p < 0.001$ compared to monetite-chitosan tablets.
b Tested using an Instron testing machine.
c Tested using a nanoindenter.

To determine the promise of hierarchical CaP materials as bone substitute materials, future studies are needed to optimize its structure and layers dimensions, investigate the effects of these materials on cellular functions, and study the tissue responses to them in vitro and in vivo. Another subject of further research includes the safety assessment of the ingredients within the hierarchical CaP-based composites. One of the major concerns is the toxicity of maleic acid, which has been shown to be a dermal and/or ocular irritant as a free acid.(65) A possible strategy to lower the concentration of free maleic acid is to neutralize it into various maleate salts.(65) The design of a pH-sensitive layer that can release the acid in a controlled dose is another strategy that could be used to reduce the toxicity during the degradation of hierarchical CaP-based composites.(66)

# 4. CONCLUSIONS

To achieve hierarchical structure in CaP materials, we devised a novel pathway to generate a layered monetite composite that can further transform into a HAp composite with a multilevel hierarchical structure. A nacre-inspired matrix composed of chitosan and maleic acid was designed to mediate the construction of an orderly layered structure. The chitosan and MAc molecules assembled into an organized complex and further guided the mineralization of monetite crystals, resulting in the formation of organized and parallel arrays of monetite platelets with a brick-and-mortar structure. By hydrolyzing the layered monetite composite in an alkali solution, hierarchical HAp with multiscale ordered structure was formed through a phase transformation under the mediation of a chitosan-MAc matrix. This hierarchical structure imparts the CaP material with improved mechanical properties and demonstrates its potential applications in hard tissue engineering. We anticipate that the approach demonstrated here will provide inspiration for biomimetic designs of advanced, mechanically robust materials for biomedical applications.

**Associated Content**: The Supporting Information is available free of charge on the ACS Publications website at DOI: 10.1021/acsbiomaterials.6b00164. Figure S1, schematic representation of the hierarchical assembly process of organized chitosan-MAc matrix based on the data in Figure 2-4; Figure S2, EDS and FTIR spectra of the layered monetite-chitosan-MAc composite; Figure S3, SEM images of the monetite crystals obtained without organic matrix, with chitosan alone, and with maleic acid alone; Figure S4, schematic representation of the formation of layered monetitechitosan-MAc composite; Figure S5, XRD and EDS spectra of the organized HAp-chitosan-MAc composite;

Figure S6, crystal structures of monetite and hydroxyapatite; Figure S7, representative photographic image of a CaP tablet prepared from layered monetite-chitosanMAc composite (PDF)

**References**:

1. Inzana, J.  A.; Olvera, D.; Fuller, S.  M.; Kelly, J.  P.; Graeve, O.  A.; Schwarz, E. M.; Kates, S. L.; Awad, H. A.3D printing of composite calcium phosphate and collagen scaffolds for bone regeneration *Biomaterials* **2014**, 35 ( 13) 4026– 4034, DOI: 10.1016/j.biomaterials.2014.01.064
2. Surmenev, R.  A.; Surmeneva, M.  A.; Ivanova, A.  A.Significance of calcium phosphate coatings for the enhancement of new bone osteogenesis-A review *Acta Biomater.* **2014**, 10 ( 2) 557– 579, DOI: 10.1016/j.actbio.2013.10.036
3. Ginebra, M.-P.; Canal, C.; Espanol, M.; Pastorino, D.; Montufar, E.  B.Calcium phosphate cements as drug delivery materials *Adv. Drug Delivery Rev.* **2012**, 64 ( 12) 1090– 1110, DOI: 10.1016/j.addr.2012.01.008
4. Akkarachaneeyakorn, K.; Li, M.; Harris, J.; Davis, S.  A.; Mann, S.Bioactive hybrid organogels based on miniemulsion synthesis of morphologically complex polymer/surfactant/calcium phosphate nanostructures *Chem. Mater.* **2014**, 26 ( 20) 5965– 5972, DOI: 10.1021/cm5027305
5. Geffers, M.; Groll, J.; Gbureck, U.Reinforcement strategies for load-bearing calcium phosphate biocements *Materials* **2015**, 8 ( 5)2700– 2717, DOI: 10.3390/ma8052700
6. Canal, C.; Ginebra, M. P.Fibre-reinforced calcium phosphate cements: a review *J. Mech. Behav. Biomed. Mater.* **2011**, 4 ( 8) 1658–1671, DOI: 10.1016/j.jmbbm.2011.06.023
7. Sugawara, A.; Asaoka, K.; Ding, S.-J.Calcium phosphate-based cements: clinical needs and recent progress *J. Mater. Chem. B* **2013**,1 ( 8) 1081– 1089, DOI: 10.1039/C2TB00061J
8. Naleway, S. E.; Porter, M. M.; McKittrick, J.; Meyers, M. A.Structural design elements in biological materials: application to bioinspiration *Adv. Mater.* **2015**, 27 ( 37) 5455– 5476, DOI: 10.1002/adma.201502403
9. Zhao, N.; Wang, Z.; Cai, C.; Shen, H.; Liang, F.; Wang, D.; Wang, C.; Zhu, T.; Guo, J.; W ang, Y.; Liu, X.; Duan, C.; Wang, H.; Mao, Y.;Jia, X.; Dong, H.; Zhang, X.; Xu, J.Bioinspi red materials: from low to high dimensional structure *Adv. Mater.* **2014**, 26 ( 41) 6994– 7017,DOI: 10.1002/adma.201401718
10. Mirkhalaf, M.; Dastjerdi, A. K.; Barthelat, F.Overcoming the brittleness of glass through bio-inspiration and micro-architecture *Nat. Commun.* **2014**, 5, 3166, DOI: 10.1038/ncomms4166

11. Bouville, F.; Maire, E.; Meille, S.; Van de Moortèle, B.; Stevenson, A. J.; Deville, S.Strong, tough and stiff bioinspired ceramics from brittle constituents *Nat. Mater.* **2014**, 13 ( 5) 508– 514, DOI: 10.1038/nmat3915

12. Le Ferrand, H.; Bouville, F.; Niebel, T. P.; Studart, A. R.Magnetically assisted slip casting of bioinspired heterogeneous composites*Nat. Mater.* **2015**, 14 ( 11) 1172– 1179, DOI: 10.1038/nmat4419

13. Wegst, U. G. K.; Bai, H.; Saiz, E.; Tomsia, A. P.; Ritchie, R. O.Bioinspired structural materials *Nat. Mater.* **2014**, 14 ( 1) 23– 36, DOI: 10.1038/nmat4089

14. Ruan, Q.; Moradian-Oldak, J.Amelogenin and enamel biomimetics *J. Mater. Chem. B* **2015**, 3 ( 16) 3112– 3129, DOI: 10.1039/C5TB00163C

15. Halgaš, R.; Dusza, J.; Kaiferová, J.; Kovácsová, L.; Markovská, N.Nanoindentation testing of human enamel and dentin *Ceramics-Silikáty* **2013**, 57 ( 2) 92– 99

16. Studart, A. R.Towards high-performance bioinspired composites *Adv. Mater.* **2012**, 24 ( 37) 5024– 5044, DOI: 10.1002/adma.201201471

17. Bai, H.; Walsh, F.; Gludovatz, B.; Delattre, B.; Huang, C.; Chen, Y.; Tomsia, A. P.; Ritchie, R. O.Bioinspired hydroxyapatite/poly(methyl methacrylate) composite with a nacre-mimetic architecture by a bidirectional freezing method *Adv. Mater.***2016**, 28, 50, DOI: 10.1002/adma.201504313

18. Li, C.; Born, A.-K.; Schweizer, T.; Zenobi-Wong, M.; Cerruti, M.; Mezzenga, R.Amyloid-hydroxyapatite bone biomimetic composites*Adv. Mater.* **2014**, 26 ( 20) 3207– 3212, DOI: 10.1002/adma.201306198

19. He, W.-X.; Rajasekharan, A. K.; Tehrani-Bagha, A. R.; Andersson, M.Mesoscopically ordered bone-mimetic nanocomposites *Adv. Mater.* **2015**, 27 ( 13) 2260– 2264, DOI: 10.1002/adma.201404926

20. He, W.; Kjellin, P.; Currie, F.; Handa, P.; Knee, C. S.; Bielecki, J.; Wallenberg, L. R.; Andersson, M.Formation of bone-like nanocrystalline apatite using self-assembled liquid crystals *Chem. Mater.* **2012**, 24 ( 5) 892– 902, DOI: 10.1021/cm201077t

21. Matlahov, I.; Iline-Vul, T.; Abayev, M.; Lee, E. M. Y.; Nadav-Tsubery, M.; Keinan-Adamsky, K.; Gray, J. J.; Goobes, G.Interfacial mineral-peptide properties of a mineral binding peptide from osteonectin and bone-like apatite *Chem. Mater.* **2015**, 27 ( 16) 5562– 5569,DOI: 10.1021/acs.chemmater.5b01696

22. Yang, Y.; Lv, X. P.; Shi, W.; Li, J. Y.; Li, D. X.; Zhou, X. D.; Zhang, L. L.8DSS-promoted remineralization of initial enamel caries in vitro*J. Dent. Res.* **2014**, 93 ( 5) 520– 4, DOI: 10.1177/0022034514522815

23. Bradt, J.-H.; Mertig, M.; Teresiak, A.; Pompe, W.Biomimetic mineralization of collagen by combined fibril assembly and calcium phosphate formation *Chem. Mater.* **1999**, 11 ( 10) 2694– 2701, DOI: 10.1021/cm991002p

24. Fan, Y.; Sun, Z.; Moradian-Oldak, J.Controlled remineralization of enamel in the presence of amelogenin and fluoride *Biomaterials***2009**, 30 ( 4) 478– 483, DOI: 10.1016/j.biomaterials.2008.10.019

25. Ruan, Q.; Zhang, Y.; Yang, X.; Nutt, S.; Moradian-Oldak, J.An amelogenin-chitosan matrix promotes assembly of an enamel-like layer with a dense interface *Acta Biomater.* **2013**, 9 ( 7) 7289– 7297, DOI: 10.1016/j.actbio.2013.04.004

26. Wu, D.; Yang, J.; Li, J.; Chen, L.; Tang, B.; Chen, X.; Wu, W.Hydroxyapatite-anchored dendrimer for in situ remineralization of human tooth enamel *Biomaterials* **2013**, 34 ( 21) 5036– 5047, DOI: 10.1016/j.biomaterials.2013.03.053

27. Li, J.; Yang, J.; Li, J.; Chen, L.; Liang, K.; Wu, W.; Chen, X.; Li, J.Bioinspired intrafibrillar mineralization of human dentine by PAMAM dendrimer *Biomaterials* **2013**, 34 ( 28) 6738– 47, DOI: 10.1016/j.biomaterials.2013.05.046

28. Chen, X.; Wang, W.; Cheng, S.; Dong, B.; Li, C. Y.Mimicking bone nanostructure by combining block copolymer self-assembly and 1D crystal nucleation *ACS Nano* **2013**, 7 ( 9) 8251– 8257, DOI: 10.1021/nn403742f

29. Hu, Y. Y.; Liu, X. P.; Ma, X.; Rawal, A.; Prozorov, T.; Akinc, M.; Mallapragada, S. K.; Schmidt-Rohr, K.Biomimetic self-assembling copolymer-hydroxyapatite nanocomposites with the nanocrystal size controlled by citrate *Chem. Mater.* **2011**, 23 ( 9) 2481– 2490, DOI: 10.1021/cm200355n

30. Li, L.; Mao, C.; Wang, J.; Xu, X.; Pan, H.; Deng, Y.; Gu, X.; Tang, R.Bio-inspired enamel repair via Glu-directed assembly of apatite nanoparticles: an approach to biomaterials with optimal characteristics *Adv. Mater.* **2011**, 23 ( 40) 4695– 4701, DOI: 10.1002/adma.201102773

31. Busch, S.Regeneration of human tooth enamel *Angew. Chem., Int. Ed.* **2004**, 43 ( 11) 1428– 1431, DOI: 10.1002/anie.200352183

32. Furuichi, K.; Oaki, Y.; Imai, H.Preparation of nanotextured and nanofibrous hydroxyapatite through dicalcium phosphate with gelatin*Chem. Mater.* **2006**, 18 ( 1) 229– 234, DOI: 10.1021/cm052213z

33. Ito, H.; Oaki, Y.; Imai, H.Selective synthesis of various nanoscale morphologies of hydroxyapatite via an intermediate phase *Cryst. Growth Des.* **2008**, 8 ( 3) 1055– 1059, DOI: 10.1021/cg070443f

34. Zou, Z.; Liu, X.; Chen, L.; Lin, K.; Chang, J.Dental enamel-like hydroxyapatite transformed directly from monetite *J. Mater. Chem.* **2012**,22 ( 42) 22637– 22641, DOI: 10.1039/c2jm35430f

35. Liu, X.; Lin, K.; Wu, C.; Wang, Y.; Zou, Z.; Chang, J.Multilevel hierarchically ordered artificial biomineral *Small* **2014**, 10 ( 1) 152– 9,DOI: 10.1002/smll.201301633

36. Addadi, L.; Joester, D.; Nudelman, F.; Weiner, S.Mollusk Shell Formation: A source of new concepts for understanding biomineralization processes *Chem. - Eur. J.* **2006**, 12 ( 4) 980– 987, DOI: 10.1002/chem.200500980

37. Levi-Kalisman, Y.; Falini, G.; Addadi, L.; Weiner, S.Structure of the nacreous organic matrix of a bivalve mollusk shell examined in the hydrated state using cryo-TEM *J. Struct. Biol.* **2001**, 135 ( 1) 8– 17, DOI: 10.1006/jsbi.2001.4372

38. Suzuki, M.; Saruwatari, K.; Kogure, T.; Yamamoto, Y.; Nishimura, T.; Kato, T.; Nagasawa , H.An acidic matrix protein, Pif, is a key macromolecule for nacre formation *Science* **2009**, 325 ( 5946) 1388– 90, DOI: 10.1126/science.1173793

39. Baskar, D.; Balu, R.; Kumar, T. S. S.Mineralization of pristine chitosan film through biomimetic process *Int. J. Biol. Macromol.* **2011**,49 ( 3) 385– 389, DOI: 10.1016/j.ijbiomac.2011.05.021

40. He, L.-H.; Yao, L.; Xue, R.; Sun, J.; Song, R.In-situ mineralization of chitosan/calcium phosphate composite and the effect of solvent on the structure *Front. Mater. Sci.* **2011**, 5 ( 3) 282– 292, DOI: 10.1007/s11706-011-0140-6

41. Li, L.; Zhao, M.; Ding, S.; Zhou, C.Rapid biomimetic mineralization of chitosan scaffolds with a precursor sacrificed method in ethanol/water mixed solution *eXPRESS Polym. Lett.* **2011**, 5 ( 6) 545– 554, DOI: 10.3144/expresspolymlett.2011.53

42. Jin, J.; Hassanzadeh, P.; Perotto, G.; Sun, W.; Brenckle, M.  A.; Kaplan, D.; Omenetto, F. G.; Rolandi, M.A biomimetic composite from solution self-assembly of chitin nanofibers in a silk fibroin matrix *Adv. Mater.* **2013**, 25 ( 32) 4482– 4487, DOI: 10.1002/adma.201301429

43. Arias, J.  L.; Fernández, M. S.Biomimetic processes through the study of mineralized shells *Mater. Charact.* **2003**, 50 ( 2–3) 189– 195,DOI: 10.1016/S1044-5803(03)00088-3

44. Sailakshmi, G.; Mitra, T.; Chatterjee, S.; Gnanamani, A.Engineering chitosan using α, ω-dicarboxylic acids—an approach to improve the mechanical strength and thermal stability *J. Biomater. Nanobiotechnol.* **2013**, 4 ( 2) 151– 164, DOI: 10.4236/jbnb.2013.42021

45. Mitra, T.; Sailakshmi, G.; Gnanamani, A.; Mandal, A.  B.Studies on cross-linking of succinic acid with chitosan/collagen *Mater. Res.***2013**, 16, 755– 765, DOI: 10.1590/S1516-14392013005000059

46. Liu, W.; Sun, S.; Cao, Z.; Zhang, X.; Yao, K.; Lu, W.  W.; Luk, K.  D.An investigation on the physicochemical properties of chitosan/DNA polyelectrolyte complexes *Biomaterials* **2005**, 26 ( 15) 2705– 11, DOI: 10.1016/j.biomaterials.2004.07.038

47. Tan, Z. H.; Jin, S. H.; Li, N. *Basic Organic Chemistry*; Scientific and Technical Documents Publishing House: Beijing, **2004**.

48. Domard, A.Determination of N-acetyl content in chitosan samples by c.d. measurements *Int. J. Biol. Macromol.* **1987**, 9 ( 6) 333– 336,DOI: 10.1016/0141-8130(87)90004-3

49. Feng, W.; Li, Y.; Ji, P.Interaction of water soluble chitosan with multiwalled carbon nanotubes *AIChE J.* **2012**, 58 ( 1) 285– 291, DOI: 10.1002/aic.12562

50. Li, W.; Liu, Y.; Perez, T.; Gunton, J.  D.; Sorensen, C.  M.; Chakrabarti, A.Kinetics of nanochain formation in a simplified model of amelogenin biomacromolecules *Biophys. J.* **2011**, 101 ( 10) 2502– 2506, DOI: 10.1016/j.bpj.2011.09.056

51. Li, W.; Chakrabarti, A.; Gunton, J.  D.Self-assembly of a bipolar model of biomacromolecules *Langmuir* **2013**, 29 ( 14) 4470– 4476, DOI: 10.1021/la4002994

52. Assis, O. B. G.; Bernardes-Filho, R.; Vieira, D. C.; Filho, S. P. C.AFM characterization of chitosan self-assembled films *Int. J. Polym. Mater.* **2002**, 51 ( 7) 633– 638, DOI: 10.1080/714975800

53. Wang, Z.; Zeng, R.; Tu, M.; Zhao, J.Synthesis, characterization of biomimetic phosphorylcholine-bound chitosan derivative and in vitro drug release of their nanoparticles *J. Appl. Polym. Sci.* **2013**, 128 ( 1) 153– 160, DOI: 10.1002/app.38151

54. Liu, J.; Zhang, L.; Wang, C.; Xu, H.; Zhao, X.Preparation and characterization of lectin-conjugated chitosan fluorescent nanoparticles*Mol. BioSyst.* **2010**, 6 ( 6) 954– 7, DOI: 10.1039/b927040j

55. Deemak, P.; Wanichwecharungruang, S.; Nonthabenjawan, R.; Jornjangjun, C.Controlling the morphology of self-assemble chitosan through derivatization *J. Polym. Res.* **2011**, 18 ( 3) 419– 424, DOI: 10.1007/s10965-010-9432-2

56. Yang, M.; Chen, G.; Zhao, Y.; Silber, G.; Wang, Y.; Xing, S.; Han, Y.; Chen, H.Mechanistic investigation into the spontaneous linear assembly of gold nanospheres *Phys. Chem. Chem. Phys.* **2010**, 12 ( 38) 11850– 11860, DOI: 10.1039/c0cp00127a

57. Zhang, H.; Fung, K.-H.; Hartmann, J.; Chan, C. T.; Wang, D.Controlled chainlike agglomeration of charged gold nanoparticles via a deliberate interaction balance *J. Phys. Chem. C* **2008**, 112 ( 43) 16830– 16839, DOI: 10.1021/jp806059a

58. Li, W.; Kanyo, I.; Kuo, C.-H.; Thanneeru, S.; He, J.pH-programmable self-assembly of plasmonic nanoparticles: hydrophobic interaction versus electrostatic repulsion *Nanoscale* **2015**, 7 ( 3) 956– 964, DOI: 10.1039/C4NR05743K

59. Max, J.-J.; Chapados, C.Infrared spectroscopy of aqueous carboxylic acids: malic acid *J. Phys. Chem. A* **2002**, 106 ( 27) 6452– 6461,DOI: 10.1021/jp014377i

60. Dosen, A.; Giese, R. F.Thermal decomposition of brushite, $CaHPO_4 2H_2O$ to monetite $CaHPO_4$ and the formation of an amorphous phase *Am. Mineral.* **2011**, 96 ( 2– 3) 368– 373, DOI: 10.2138/am.2011.3544

61. Xiao, J.; Zhu, Y.; Ruan, Q.; Liu, Y.; Zeng, Y.; Xu, F.; Zhang, L.Biomacromolecule and surfactant complex matrix for oriented stack of 2-dimensional carbonated hydroxyapatite nanosheets as alignment in calcified tissues *Cryst. Growth Des.* **2010**, 10 ( 4) 1492– 1499, DOI: 10.1021/cg9001016

62. Wang, M.; Gao, J.; Shi, C.; Zhu, Y.; Zeng, Y.; Wang, D.Facile one-pot synthesis of oriented pure hydroxyapatite with hierarchical architecture by topotactic conversion *Cryst. Growth Des.* **2014**, 14 ( 12) 6459– 6466, DOI: 10.1021/cg5013044

63. Panzavolta, S.; Bracci, B.; Focarete, M. L.; Gualandi, C.; Bigi, A.Fiber reinforcement of a biomimetic bone cement *J. Mater. Sci.: Mater. Med.* **2012**, 23 ( 6) 1363– 1370, DOI: 10.1007/s10856-012-4618-2

64. Ni, G. X.; Choy, Y. S.; Lu, W. W.; Ngan, A. H. W.; Chiu, K. Y.; Li, Z. Y.; Tang, B.; Luk, K. D. K.Nano-mechanics of bone and bioactive bone cement interfaces in a load-bearing model *Biomaterials* **2006**, 27 ( 9) 1963– 1970, DOI: 10.1016/j.biomaterials.2005.09.044

65. Cosmetic Ingredient Review Expert PanelFinal report on the safety assessment of Maleic Acid *Int. J. Toxicol.* **2007**, 26 ( S2) 125– 130,DOI: 10.1080/10915810701351251

66. Sen, M.; Uzun, C.; Guven, O.Controlled release of terbinafine hydrochloride from pH sensitive poly(acrylamide/maleic acid) hydrogels*Int. J. Pharm.* **2000**, 203 ( 1– 2) 149– 157, DOI: 10.1016/S0378-5173(00)00449-X